Cauchy-Riemann beams

H. M. Moya-Cessa ©, I. Ramos-Prieto ©,* D. Sánchez-de-la-Llave ©, U. Ruíz ©, V. Arrizón, and F. Soto-Eguibar ©

Instituto Nacional de Astrofísica Óptica y Electrónica, Calle Luis Enrique Erro No. 1, Santa María Tonantzintla, Puebla 72840, Mexico

Leveraging operator techniques, we address the paraxial wave equation governing a field formed by the multiplication of a Gaussian function and an entire function; notably, the latter adheres to the Laplace equation, $\nabla_\perp^2 f(x+iy) = 0$, a direct consequence of satisfying the Cauchy-Riemann equations. Our theoretical and experimental exploration brings to light the intrinsic rotation of this field during propagation, elucidated by the incorporation of the quantum (Bohm) potential. This straightforward result holds promise, enabling the analytical deduction of the Fraunhofer or Fresnel diffraction pattern. Essentially, it simplifies the extraction of the Fresnel or Fourier transform from a function satisfying the Cauchy-Riemann equations.

I. INTRODUCTION

Over the past five decades, the scientific community has seen the emergence of numerous solutions to the paraxial equation, which are crucial in the study of wave propagation. These solutions have explored various coordinate systems, ranging from specific field forms to more general ones. While examples of these solutions can be found in a wide range of references [1–16], they by no means constitute an exhaustive account of the field. Two distinctive approaches are presented in Refs. [17,18]. In the former, a method is presented for calculating trajectories of optical vortices of Gaussian beams in terms of paraxial modes. Meanwhile, in the latter, the approach involves breaking down the paraxial equation into a system of two equations. The field's magnitude and phase are considered as separate entities and a structurally stable ansatz is proposed for the field intensity. The resulting solution encompasses functions wherein the complex amplitude can be represented by a complex entire function multiplied by a Gaussian distribution.

In this paper, we introduce an approach aimed at deriving closed-form solutions to the paraxial equation. Our approach builds upon the well-established fact that entire functions are solutions to the Laplace equation. The solutions we present are equivalent to those presented by Abramochkin *et al.* [18], where complex amplitudes of fields were initially represented by entire functions multiplied by a real Gaussian function at $z = 0$. Leveraging concepts from quantum optics operators, we formulate closed-form expressions that precisely describe the propagation of these fields. One intriguing characteristic of these beams is their innate ability to undergo self-transformation during a Fourier transform operation, provided an axis rotation is allowed, i.e., the function that describes the field at the plane $z = 0$ and its Fourier transform are scaled and rotated versions of each other. To shed light

on this phenomenon, we propose a fresh interpretation of the field's rotation based on the quantum Bohm potential. Our innovative approach not only contributes to a deeper understanding of these wave fields but also extends their practical applications. By providing a new perspective on their behavior and properties, our research aims to enhance comprehension and open up new avenues for utilizing these wave phenomena across various fields.

It is well known that an analytic function $f(x + iy)$ satisfies the Cauchy-Riemann equations and, in turn, is a solution of the Laplace equation, i.e., $\nabla_\perp^2 f(x+iy) = 0$, with $\nabla_\perp^2 = \frac{\partial^2}{\partial_x^2} + \frac{\partial^2}{\partial_y^2}$ denoting the transverse component of the Laplacian [19–21]. Undoubtedly, when the function f exhibits multivalued behavior within specific regions or at certain points in the complex plane, it remains eligible for classification as an analytic function, subject to specific limitations. In light of these considerations, and in the context of optical scalar fields, we have chosen to designate such fields as Cauchy-Riemann beams (CRBs). These beams denote functions that are differentiable within a certain region, potentially spanning the entire complex plane, and satisfying the Cauchy-Riemann equations. It is worth noting that Abramochkin *et al.* (among others, e.g., Kotlyar *et al.* [22]) had already observed indications of these fields, initially labeling them as spiral-type beams [18,23].

We organize our work as follows: Section II delves into the theoretical foundations of Cauchy-Riemann beams, discussing the paraxial equation and the concept of square integrability associated with the Cauchy-Riemann equations. These discussions encompass the analytical properties and experimental evidence linked to Cauchy-Riemann beams. Moreover, this section examines the Fraunhofer and Fresnel diffraction phenomena exhibited by Cauchy-Riemann beams. In Sec. III, we introduce the quantum Bohm potential and its mathematical formulation to explain the rotation of Cauchy-Riemann beams. Finally, Sec. IV presents the concluding remarks of the research, summarizing the key findings and their implications.

*iran@inaoep.mx

043528-1

II. CAUCHY-RIEMANN BEAMS

Let $f(x + iy)$ be a solution to the Laplace equation; thus, this function is a solution to the paraxial equation

$$\nabla_\perp^2 E(x, y, z) + 2ik \frac{\partial E(x, y, z)}{\partial z} = 0, \qquad (1)$$

where $k = \frac{2\pi}{\lambda}$ is the wave number.

Certainly, similar to Bessel beams [1], these solutions are not physically realizable because they are not square integrable. In light of this, drawing inspiration from Bessel-Gauss beams [2], we seek a generalized version that incorporates a Gaussian factor to render the field square integrable. It is essential to emphasize that not all analytic functions, when multiplied by such Gaussian factors, become square integrable. To achieve this goal, we write the paraxial equation as a Schrödinger-like equation, $\frac{\partial E(x,y,z)}{\partial z} = \frac{i}{2k}\nabla_\perp^2 E(x, y, z)$, whose formal solution can be written as $E(x, y, z) = \exp(i\frac{z}{2k}\nabla_\perp^2)E(x, y, 0)$, being $E(x, y, 0)$ the initial field at $z = 0$. In the subsequent analysis, we adopt an approach involving operators less commonly employed in physical optics [21,24]. This approach, however, proves advantageous in obtaining solutions to the paraxial equation when an initial condition is provided. As a result, in Cartesian coordinates, the field at location z is calculated as

$$E(x, y, z) = \exp\left[-\frac{i}{2k}z\left(\hat{p}_x^2 + \hat{p}_y^2\right)\right]E(x, y, 0), \qquad (2)$$

where we have introduced the operators $\hat{p}_x = -i\frac{\partial}{\partial x}$ and $\hat{p}_y = -i\frac{\partial}{\partial y}$, which obey the following commutation relations: $[x, \hat{p}_x] = [y, \hat{p}_y] = i$ and $[x, y] = [x, \hat{p}_y] = [y, \hat{p}_x] = [\hat{p}_x, \hat{p}_y] = 0$. Now, we write the initial condition as $E(x, y, 0) = \exp[-g(x^2 + y^2)]f(x + iy)$, with g taking values in the complex number domain ($g \in \mathbb{C}$). By substituting this initial condition into Eq. (2), we obtain $E(x, y, z) = \exp[-\frac{i}{2k}z(\hat{p}_x^2 + \hat{p}_y^2)]\exp[-g(x^2 + y^2)]f(x + iy)$. As a subsequent step, we introduce the identity operator $\hat{I}$, expressed as $\hat{I} = e^{\frac{i}{2k}z(\hat{p}_x^2 + \hat{p}_y^2)}e^{-\frac{i}{2k}z(\hat{p}_x^2 + \hat{p}_y^2)}$. Therefore, the equation that describes the field $E(x, y, z)$, incorporating this identity operator, is given as follows,

$$E(x, y, z) = \exp\left[-\frac{i}{2k}z\left(\hat{p}_x^2 + \hat{p}_y^2\right)\right]\exp[-g(x^2 + y^2)]$$

$$\times \exp\left[\frac{i}{2k}z\left(\hat{p}_x^2 + \hat{p}_y^2\right)\right]$$

$$\times \exp\left[-\frac{i}{2k}z\left(\hat{p}_x^2 + \hat{p}_y^2\right)\right]f(x + iy). \qquad (3)$$

The previous equation has two fundamental ingredients. The first one is that the set of operators $\hat{p}_q^2$, q^2, and $q\hat{p}_q + \hat{p}_q q$ (with $q = x, y$) is closed under commutation. Consequently, by using the Hadamard lemma [25,26], it is possible to demonstrate that $e^{-i\frac{Z}{2}\hat{p}_q^2}e^{-gq^2}e^{i\frac{Z}{2}\hat{p}_q^2} = e^{-g[q^2 - Z(q\hat{p}_q + \hat{p}_q q) + Z^2\hat{p}_q^2]}$, with $q = x, y$, where we rescaled the propagation distance to $Z = z/k$. The second, and more significant, aspect (which serves as the inspiration for the work's title), is that an analytic function $f(x + iy)$ satisfies the Cauchy-Riemann equations, and acts as an eigenfunction of the transverse Laplacian operator, with

an eigenvalue equal to zero. Therefore, from Eq. (3), it follows that

$$E(x, y, z) = e^{-g[x^2 - Z(x\hat{p}_x + \hat{p}_x x) + Z^2\hat{p}_x^2]}$$

$$\times e^{-g[y^2 - Z(y\hat{p}_y + \hat{p}_y y) + Z^2\hat{p}_y^2]}f(x + iy). \qquad (4)$$

The commutation-closed characteristic of the operator set permits the factorization of the exponential operator in the aforementioned equation [27],

$$e^{-g[q^2 - Z(q\hat{p}_q + \hat{p}_q q) + Z^2\hat{p}_q^2]} = e^{\alpha(z)q^2}e^{\beta(z)(q\hat{p}_q + \hat{p}_q q)}e^{\gamma(z)\hat{p}_q^2}, \qquad (5)$$

where $\alpha(z) = \frac{-g}{w(z)}$, $\beta(z) = -\frac{\pi}{4} - \frac{i}{2}\ln[iw(z)]$, and $\gamma(z) = -\frac{gZ^2}{w(z)}$, with $w(z) = 2igZ + 1$, for $q = x, y$ respectively. Therefore, as a direct consequence of $e^{\gamma(z)(\hat{p}_x^2 + \hat{p}_y^2)}f(x + iy) = f(x + iy)$, by substituting Eq. (5) into Eq. (4), we can represent the solution as $E(x, y, z) = e^{\alpha(z)(x^2 + y^2)}e^{\beta(z)(x\hat{p}_x + \hat{p}_x x + y\hat{p}_y + \hat{p}_y y)}f(x + iy)$. Finally, the last exponential in the above equation is the well-known squeeze operator that may be applied to the analytic function to give

$$E(x, y, z) = \frac{\exp\left[-\frac{g(x^2 + y^2)}{w(z)}\right]}{w(z)}f\left(\frac{x + iy}{w(z)}\right). \qquad (6)$$

The preceding result provides a comprehensive understanding of the propagation of fields that satisfy the Cauchy-Riemann equations, which are modulated at $z = 0$ by either a Gaussian function, a quadratic-phase function, or both. This representation proves to be versatile and generic, rendering it suitable for a wide array of scenarios in which these equations are applicable. As illustrative examples, we consider the entire functions $f_1(x + iy) = \cos[\frac{2\pi}{T}(x + iy)]$ and $f_2(x + iy) = J_1[\frac{2\pi}{T}(x + iy)]$, where $J_1(\zeta)$ is the Bessel function with $n = 1$. Figure 1 shows both the numerical and the experimental intensity distribution of the fields given by Eq. (6), on the planes $z = 0.0$ m and $z = 0.5$ m, with the parameters $T = 0.0008$ m, the x and y coordinates ranging from -0.2 to 0.2 cm, and the constant $g = 1.25 \times 10^7$ m^{-2}.

A. Experimental setup

For the generation of experimental fields, we utilize a synthetic phase hologram capable of encoding any complex field $s(x, y) = a(x, y)\exp[i\phi(x, y)]$, where $a(x, y)$ and $\phi(x, y)$ represent the amplitude and phase modulation, respectively. The synthetic phase hologram is given by [28]

$$h(x, y) = \exp\{if[a(x, y)]\sin[\phi(x, y)]\}. \qquad (7)$$

For instance, the function $f[a(x, y)]$ can be evaluated through the relationship $J_1 f[a(x, y)] = Aa(x, y)$. The maximum value of A that satisfies Eq. (7) is $A = 0.5819$, corresponding to the peak value of the first-order Bessel function $J_1(\alpha)$, which, in turn, occurs at $\alpha = 1.84$. By using a $4f$-optical system, shown in Fig. 2, we displayed the corresponding synthetic phase hologram on a phase-only spatial light modulator (PLUTO, Holoeye GmbH), which is impinged by a collimated He-Ne laser ($\lambda = 633$ nm), to generate the different reported fields. The field intensities at $z = 0.5$ m, depicted in Figs. 1(c) and 1(g), demonstrate a rotational difference concerning the field intensities shown in Figs. 1(a) and 1(e) at $z = 0.0$ m.

FIG. 2. The experimental setup employed for synthesizing a desired optical field involves a linearly polarized He-Ne laser ($\lambda =$ 633 nm) directed onto a spatial light modulator (SLM). The SLM exhibits the required synthetic phase hologram. By utilizing a $4f$-optical system and a binary spatial filter (SF), we can selectively isolate one of the diffracted orders from the synthetic phase hologram. The chosen order carries the desired complex field spatial distribution, allowing for a precise synthesis of the desired optical field after an optical Fourier transform operation.

Comparing the above equation with the field predicted by the Fresnel integral of diffraction, one can deduce that the field given by Eq. (6) at the plane $Z = 0$, with g_R taking a real positive value, is a self-transforming field under the Fourier transform operator. In general, the field at $Z = 1/(2g_I)$ is a scaled version of the field at $Z = 0$ (without the thin lens factor) and undergoes an axis rotation of $-\pi/2$ rad. An interesting example arises when $g_I = g_R$. In this case, the field at $Z = 1/(2g_I)$ is a replica of the field at $Z = 0$ (without the quadratic phase term) with an axis rotation of $-\pi/2$ rad. Next, we analyze the field properties in the far-field region.

C. Fraunhofer diffraction

Continuing along the same line of thought, when the condition $2Z|g_R + ig_R| \gg 1$ is met, indicating far-field diffraction, and replacing $Z = \lambda z/2\pi$, after some algebraic manipulations, Eq. (6) can be reformulated as follows,

$$E(x, y, z) = -\frac{i\pi}{\lambda z g^*} \exp\left[\frac{i\pi(x^2+y^2)}{\lambda z} - \frac{\pi^2}{g^*}\frac{(x^2+y^2)}{\lambda^2 z^2}\right]$$
$$\times f\left[\frac{\pi}{\lambda z}\left(-\frac{ix}{g^*} + \frac{y}{g}\right)\right], \tag{9}$$

where the symbol * denotes the complex conjugate. Therefore, comparing the above equation with the field given by the Fraunhofer integral of diffraction, one can conclude that the Fourier transform of the field described by Eq. (6) at the plane $Z = 0$ is given by

$$\mathcal{F}\{e^{-g(x^2+y^2)}f(x+iy)\} = \frac{\pi}{g^*} \exp\left[-\frac{\pi^2}{g^*}\left(v_x^2 + v_y^2\right)\right]$$
$$\times f\left[\pi\left(-\frac{iv_x}{g^*} + \frac{v_y}{g}\right)\right], \tag{10}$$

where v_x and v_y are the spatial frequencies in Cartesian coordinates. Aside from the axis rotation of the entire function, it is remarkable that this family of functions is self-transforming under the Fourier transform operator.

Finally, we note that the total axis rotation the field undergoes as it propagates across the whole z axis is $-\pi$ rad. However, the axis rotation as the field propagates from $z = 0$
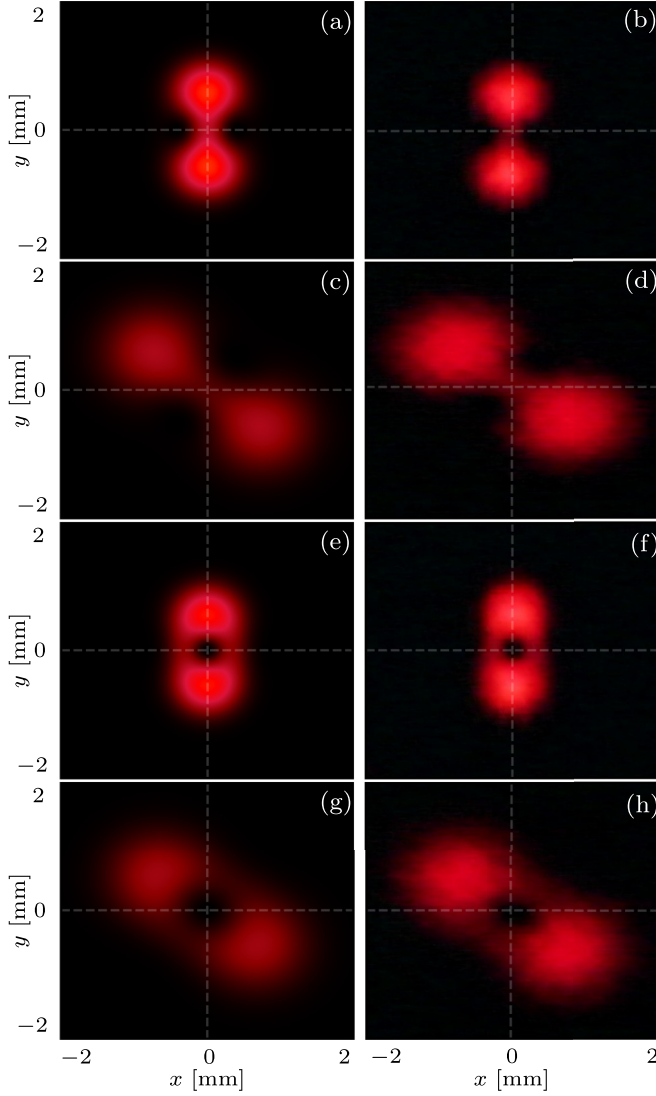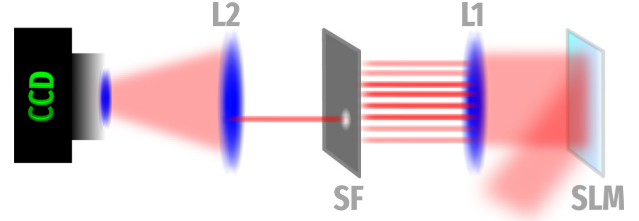
FIG. 1. Intensity distribution of the field with $f(x + iy) = \cos[\frac{2\pi}{T}(x + iy)]$ at $z = 0.0$ m, (a) theoretical, and (b) experimental; in (c) and (d) we present the same situation, but with the propagation distance $z = 0.5$ m. (e) and (f) depict the theoretical and experimental results, respectively, when $f(x + iy) = J_1[\frac{2\pi}{T}(x + iy)]$ at $z = 0.0$ m; and at $z = 0.5$ m we have (g) and (h). The parameters are $g = 1.25 \times 10^7$ m^{-2}, $T = 0.0008$ m, and $\lambda = 633$ nm, all within a viewing window in millimeters.

B. Fresnel diffraction

To examine in greater detail the field distribution and its characteristics when the parameter g takes complex values, i.e., $g = g_R + ig_I$ (with $g_R > 0$, $g_I \geqslant 0$), the quadratic phase term associated to g_I can be regarded as a thin lens with a focal length of $1/2g_I$. In this sense, the field at $Z = 1/2g_I$ is determined according to Eq. (6) as follows:

$$E\left(x, y, \frac{1}{2g_I}\right) = -\frac{ig_I}{g_R} \exp\left[-\frac{g_I^2}{g_R}(x^2+y^2)\right]$$
$$\times \exp\left[ig_I(x^2+y^2)\right]f\left[-\frac{ig_I}{g_R}(x+iy)\right]. \tag{8}$$

up to the far-field region is $-\pi/2$ rad, for $g_I = 0$, and tends to $-\pi$ rad when g_I is much larger than g_R. For the case of negative g_I, the field rotates less than $-\pi/2$ rad as it propagates from $z = 0$ to the far-field zone. In general, the rate of rotation of the axis is not linear with z, being zero in the far field.

III. BOHM FORMALISM

It is well known that Airy waves bend while they propagate [29–32]. Furthermore, their Bohm trajectories [33] may be demonstrated in hydrodynamic systems [34], where the quantum potential is linear. The rotation suffered by the Cauchy-Riemann beams during propagation may also be attributed to the so-called quantum potential. In the Bohm formalism, we have that by writing

$$E(x, y, z) = A(x, y, z) \exp[iS(x, y, z)], \qquad (11)$$

the differential equations that obey the amplitude and the phase are $\frac{1}{2}S_x^2 + \frac{1}{2}S_y^2 + V_B + S_t = 0$, where, as we are dealing with free-space propagation, we have omitted the standard potential, and

$$\frac{\partial A}{\partial z} + S_x \frac{\partial A}{\partial x} + S_y \frac{\partial A}{\partial y} + \frac{1}{2}(S_{xx}A + S_{yy}A) = 0, \qquad (12)$$

where the subindices represent partial derivatives, and the dependence on x, y, z has been omitted. The quantum or Bohm potential is

$$V_B(x, y, z) = -\frac{1}{2} \frac{\nabla_\perp^2 A(x, y, z)}{A(x, y, z)}. \qquad (13)$$

The Bohm potential for the Cauchy-Riemann beams, Eq. (6), is given by

$$Q(x, y, z) = \frac{2g}{w(z)} - \frac{2g^2(x^2 + y^2)}{w(z)^2} + \frac{2g(x + iy)}{w(z)^2} \frac{f'\left(\frac{x+iy}{w(z)}\right)}{f\left(\frac{x+iy}{w(z)}\right)}, \qquad (14)$$

where the prime denotes derivative with respect to the argument.

For the functions used in Fig. 1, namely cosine and Bessel functions, the quantum potential exists and produces the effect of rotating the field, but its expressions are complex. A function of the form $f(x + iy) = \exp[\eta(x + iy)^2]$, besides delivering a simple quantum potential, that produces the same rotating effect as seen in Fig. 3 theoretically and experimentally, is a good example to show that not any entire function has square-integrable properties, as for $|\eta| \geqslant |g|$ the field has infinite energy. The propagated field in this case is given by

$$E(x, y, z) = \frac{e^{-g\frac{x^2+y^2}{R(z)}}e^{-i\Phi_G}}{R(z)} e^{\eta \frac{(x+iy)^2}{R^2(z)}e^{-2i\Phi_G}} e^{-i\Phi_G}, \qquad (15)$$

where $\Phi_G = \arctan(2gZ)$ is the so-called Gouy phase, which may explained with the help of the quantum Bohm potential [35] and $R(z) = |w(z)|$. From the above equation, we get

$$A(x, y, z) = \frac{\exp\left[-\frac{g(x^2+y^2)\cos\Phi_G}{R(z)}\right]}{R}$$

$$\times \exp\left[\frac{\eta[(x^2 - y^2)\cos(2\Phi_G) + 2xy\sin(2\Phi_G)]}{R^2(z)}\right], \qquad (16)$$
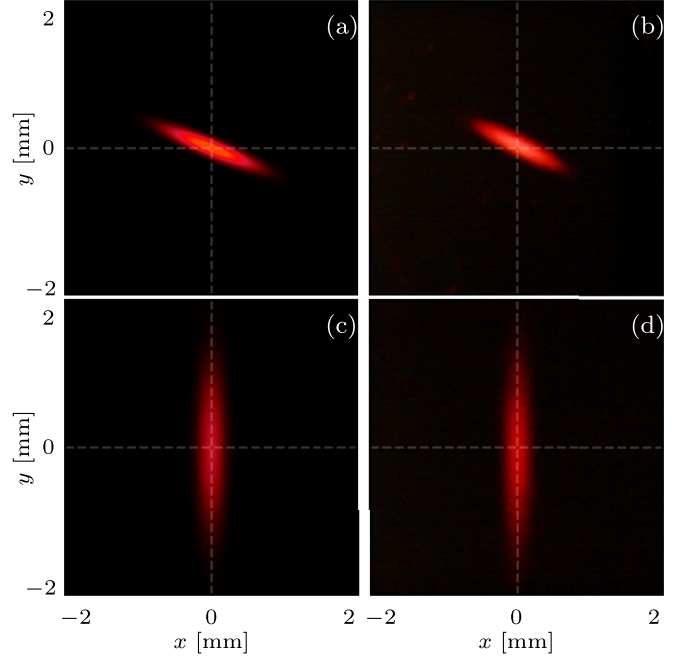

FIG. 3. The left column represents the intensity of the field for $f(x + iy) = \exp[\eta(x + iy)^2]$, while the right column shows the experimental results. The parameters used in the experimental setup are as follows: $T = 8 \times 10^{-4}$ m, $g = \frac{12}{T^2}(1 + i)$, and $\eta = \frac{2}{3}g$. (a) and (b) depict the intensity distribution at $z = 0.0$ m, and (c) and (d) display the intensity at $z = 0.45$ m using Eq. (6).

and

$$S(x, y, z) = -\Phi_G + \frac{g(x^2 + y^2)\sin\Phi_G}{R(z)}$$

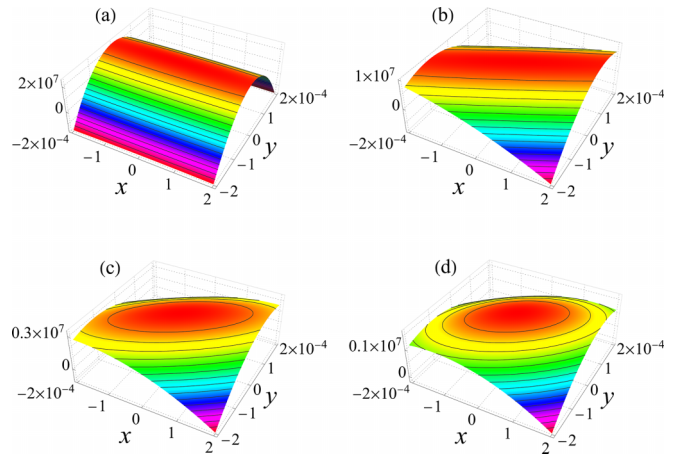$$+ \frac{\eta[2xy\cos(2\Phi_G) - (x^2 - y^2)\sin(2\Phi_G)]}{R^2(z)}, \qquad (17)$$

FIG. 4. The Bohm potential $V_B(x, y)$ for the Cauchy-Riemann field given in (18) at distances z from 0.0 to 1.5×10^{-7} in increments of 0.5×10^{-7}: (a) $z = 0.0$, (b) $z = 0.5 \times 10^{-7}$, (c) $z = 1.0 \times 10^{-7}$, and (d) $z = 1.5 \times 10^{-7}$. The independent variables, x and y, vary from -2.0×10^{-4} to 2.0×10^{-4}, and the range of the Bohm potential is scaled in each of the figures. The values of the parameters are $g = 1.25 \times 10^7$ and $\eta = 1.0 \times 10^7$. The colors, being scaled, are solely to emphasize the "rotation" of the Bohm's potential.

from where we readily may find the quantum potential

$$V_B = -2(x^2 + y^2)\left(\frac{\eta^2}{R^4} + \frac{g^2}{R^2}\cos^2\Phi_G\right) + \frac{2g}{R}\cos\Phi_G$$
$$+ \frac{4g\eta}{R^3}\cos\Phi_G[\cos(2\Phi_G)(x^2 - y^2) + 2xy\sin(2\Phi_G)],$$
(18)

where we have omitted the dependence on z of the function $R(z)$. The Bohm potential, responsible for the rotation of the beams, is plotted in Fig. 4 for several propagation distances. Since we are considering propagation in free space, there is no *potential* (index of refraction) that may affect the electromagnetic field. Therefore, the rotation is produced by the quantum potential, that in the case of Eq. (18) resembles a gradient-index (GRIN) medium [36,37] which depends quadratically on the positions x and y and changes with the propagation distance.

IV. CONCLUSIONS

We have demonstrated a solution to the paraxial equation using an unconventional approach in the field of paraxial optics, specifically by employing the operator technique from quantum mechanics, and more precisely, quantum optics; this approach is grounded in the fact that $\nabla_\perp^2 f(x + iy) = 0$. Consequently, it follows that $f(x + iy)$ serves as an eigenfunction of the Laplacian operator in two dimensions with an eigenvalue zero, an attribute stemming from $f(x + iy)$ satisfying the Cauchy-Riemann equations. In addition, we have explored specific cases of the general result provided by Eq. (6), which holds significant interest in the field of diffractive optics. It allows for the straightforward determination of Fresnel and Fraunhofer diffraction for a wide range of initial conditions when considering g in the complex number domain. It is worth noting that experimental evidence supports the observation that this solution exhibits rotation. Furthermore, we have developed the Bohm quantum potential to elucidate the reason behind the observed rotation in these solutions.

Such Cauchy-Riemann beams could be helpful in optical trapping systems [38]. Elucidation of their rotational behavior and unique phase structures can contribute significantly to greater precision in the manipulation of microscopic particles within such arrangements. This task is particularly relevant in the context of optical traps, because the paraxial equation characterizes the behavior of light near the optical axis of a thin lens.

[1] J. Durnin, Exact solutions for nondiffracting beams. I. The scalar theory, J. Opt. Soc. Am. A **4**, 651 (1987).

[2] F. Gori, G. Guattari, and C. Padovani, Bessel-Gauss beams, Opt. Commun. **64**, 491 (1987).

[3] C. Caron and R. Potvliege, Bessel-modulated Gaussian beams with quadratic radial dependence, Opt. Commun. **164**, 83 (1999).

[4] J. C. Gutiérrez-Vega, M. D. Iturbe-Castillo, and S. Chávez-Cerda, Alternative formulation for invariant optical fields: Mathieu beams, Opt. Lett. **25**, 1493 (2000).

[5] Y. Cai, X. Lu, and Q. Lin, Hollow Gaussian beams and their propagation properties, Opt. Lett. **28**, 1084 (2003).

[6] A. P. Kiselev, New structures in paraxial Gaussian beams, Opt. Spectrosc. **96**, 479 (2004).

[7] M. A. Bandres and J. C. Gutiérrez-Vega, Ince–Gaussian beams, Opt. Lett. **29**, 144 (2004).

[8] M. A. Bandres, J. C. Gutiérrez-Vega, and S. Chávez-Cerda, Parabolic nondiffracting optical wave fields, Opt. Lett. **29**, 44 (2004).

[9] J. C. Gutiérrez-Vega and M. A. Bandres, Helmholtz–Gauss waves, J. Opt. Soc. Am. A **22**, 289 (2005).

[10] M. A. Bandres and J. C. Gutiérrez-Vega, Airy-Gauss beams and their transformation by paraxial optical systems, Opt. Express **15**, 16719 (2007).

[11] V. V. Kotlyar, R. V. Skidanov, S. N. Khonina, and V. A. Soifer, Hypergeometric modes, Opt. Lett. **32**, 742 (2007).

[12] A. P. Kiselev, Localized light waves: Paraxial and exact solutions of the wave equation (a review), Opt. Spectrosc. **102**, 603 (2007).

[13] E. Karimi, G. Zito, B. Piccirillo, L. Marrucci, and E. Santamato, Hypergeometric-Gaussian modes, Opt. Lett. **32**, 3053 (2007).

[14] M. A. Bandres and J. C. Gutiérrez-Vega, Cartesian beams, Opt. Lett. **32**, 3459 (2007).

[15] M. A. Bandres and J. C. Gutiérrez-Vega, Circular beams, Opt. Lett. **33**, 177 (2008).

[16] M. A. Bandres and J. C. Gutiérrez-Vega, Elliptical beams, Opt. Express **16**, 21087 (2008).

[17] F. S. Roux, Paraxial modal analysis technique for optical vortex trajectories, J. Opt. Soc. Am. B **20**, 1575 (2003).

[18] E. Abramochkin and V. Volostnikov, Spiral-type beams, Opt. Commun. **102**, 336 (1993).

[19] J. W. Brown and R. V. Churchill, *Complex Variables and Applications*, 8th ed. (McGraw-Hill, Boston, MA, 2009).

[20] W. P. Schleich, I. Tkáčová, and L. Happ, Insights into complex functions, in *Sketches of Physics: The Celebration Collection*, edited by R. Citro, M. Lewenstein, A. Rubio, W. P. Schleich, J. D. Wells, and G. P. Zank (Springer International Publishing, Cham, 2023), pp. 127–159.

[21] I. Ramos-Prieto, D. Sánchez-de-la-Llave, U. Ruíz, V. Arrizón, F. Soto-Eguibar, and H. M. Moya-Cessa, Cauchy-Riemann beams in GRIN media, arXiv:2311.09541.

[22] V. V. Kotlyar, A. A. Kovalev, and E. G. Abramochkin, Topological charge of propagation-invariant laser beams, Photonics **10**, 915 (2023).

[23] E. Abramochkin and V. Volostnikov, Spiral-type beams: optical and quantum aspects, Opt. Commun. **125**, 302 (1996).

[24] D. Stoler, Operator methods in physical optics, J. Opt. Soc. Am. **71**, 334 (1981).

[25] W. Rossmann, *Lie Groups: An Introduction Through Linear Groups* (Oxford University Press, Oxford, U.K., 2002).

[26] B. C. Hall, *Lie Groups, Lie Algebras, and Representations* (Springer, New York, 2013).

[27] J. Wei and E. Norman, On global representations of the solutions of linear differential equations as a product of exponentials, Proc. Am. Math. Soc. **15**, 327 (1964).

[28] V. Arrizón, U. Ruiz, R. Carrada, and L. A. González, Pixelated phase computer holograms for the accurate encoding of scalar complex fields, J. Opt. Soc. Am. A **24**, 3500 (2007).

[29] G. A. Siviloglou, J. Broky, A. Dogariu, and D. N. Christodoulides, Observation of accelerating Airy beams, Phys. Rev. Lett. **99**, 213901 (2007).

[30] G. G. Rozenman, M. Zimmermann, M. A. Efremov, W. P. Schleich, L. Shemer, and A. Arie, Amplitude and phase of wave packets in a linear potential, Phys. Rev. Lett. **122**, 124302 (2019).

[31] S. A. Hojman, F. A. Asenjo, H. M. Moya-Cessa, and F. Soto-Eguibar, Bohm potential is real and its effects are measurable, Optik **232**, 166341 (2021).

[32] G. Silva-Ortigoza and J. Ortiz-Flores, Properties of the Airy beam by means of the quantum potential approach, Phys. Scr. **98**, 085106 (2023).

[33] D. Bohm, A suggested interpretation of the quantum theory in terms of "hidden" variables. I, Phys. Rev. **85**, 166 (1952).

[34] G. G. Rozenman, D. I. Bondar, W. P. Schleich, L. Shemer, and A. Arie, Observation of Bohm trajectories and quantum potentials of classical waves, Phys. Scr. **98**, 044004 (2023).

[35] H. M. Moya-Cessa, S. A. Hojman, F. A. Asenjo, and F. Soto-Eguibar, Bohm approach to the Gouy phase shift, Optik **252**, 168468 (2022).

[36] A. Urzúa, I. Ramos-Prieto, E. Soto-Eguibar, V. Arrizon, and H. Moya-Cessa, Light propagation in inhomogeneous media, coupled quantum harmonic oscillators and phase transitions, Sci. Rep. **9**, 16800 (2019).

[37] F. A. Asenjo, S. A. Hojman, H. M. Moya-Cessa, and F. Soto-Eguibar, Propagation of light in linear and quadratic grin media: The Bohm potential, Opt. Commun. **490**, 126947 (2021).

[38] A. Ashkin, J. M. Dziedzic, and T. Yamane, Optical trapping and manipulation of single cells using infrared laser beams, Nature (London) **330**, 769 (1987).